Research Square

Preprints are preliminary reports that have not undergone peer review.
They should not be considered conclusive, used to inform clinical practice,
or referenced by the media as validated information.

Oxidation of Cellulose by the Fenton Reaction: Application to Superabsorbents Hydrogels

Tsague Fabien Lucioni
Assonfack Hermann Lekane
SAHA TCHINDA Jean-Bosco SAHA TCHINDA
Nnanga Guissele Hubert Justin
Mewoli Armel Edwige
Cheumani Yona Arnaud Maxime
Chimeni-Yomeni DESIRE Désiré
desireyck@yahoo.fr

Université de Yaoundé I: Universite de Yaounde I https://orcid.org/0000-0002-8183-4888
Ndikontar Kor Maurice

Research Article

Keywords: Cellulose, Fenton reaction, hydrogels SAPs, Water absorption capacity

Posted Date: November 25th, 2026

DOI: https://doi.org/10.21203/rs.3.rs-11693056/v1

License: This work is licensed under a Creative Commons Attribution 4.0 International License.
Read Full License

Oxidation of Cellulose by the Fenton Reaction: Application to Superabsorbents Hydrogels.

Fabien Lucioni Tsague [1] , Hermann Lekane Assonfack [1] , Jean-Bosco Saha Tchinda [1] ,Hubert Justin Guissele Nnanga [1] , Armel Edwige Mewoli [3] , Arnaud Maxime Cheumani Yona [1] , Desire Chimeni-Yomeni [1,2*] , Kor Maurice Ndikontar [1]

[1] *Macromolecular Research Team, Faculty of Science, University of Yaoundé 1, P.O 812, Yaounde, Cameroon.*

[2] *Analytical Laboratory, LABPLAS, Saint Julie, Montréal, QC J3E1Z6, Canada.*

[3] *National Advanced School of Engineering, University of Yaounde 1, Cameroun (ENSPY)*

lucionitsague@gmail.com (Fist author) +237(670810811)

assonfackherman@yohoo.com

saha_jb@yahoo.fr

guissele.nnanga@facsciences-uy1.cm

mewoliarmel@yahoo.fr

acheumani@gmail.com

dchimeniyomeni@laplas.com (Corresponding author): Phone +1(581) 578-651)

mndikontar@yahoo.com

Abstract: Hydrogels were synthesized from oxidized cellulose obtained via a Fenton reaction in the presence of sodium chloride (NaCl) as an alkaline metal salt, reinforced with starch. Compared to native cellulose, the oxidized form underwent partial depolymerization, enabling the introduction of carboxyl (–COOH) groups. This functionalization promoted the formation of a three-dimensional network through covalent ionic crosslinking. The resulting structure was confirmed using Fourier transform infrared spectroscopy (FT-IR), scanning electron microscopy (SEM), X-ray diffraction (XRD), and thermogravimetric/differential thermogravimetric (TGA–DTG) analysis. Due to their pronounced hydrophilicity, the hydrogels achieved a maximum water absorption capacity of 691 g of water per gram of gel, still below that of commercial synthetic superabsorbent SAPs (~1000 g/g). In saline medium (0.9% NaCl/wt.) the maximum water absorption reached 113 g/g, exceeding commercial SAPs (40–50 g/g) by more than two-fold. Equilibrium swelling ratios in distilled water and biological fluids such as D-glucose or urea solutions ranged from 691 to 375 g/g, and from 198 to 95 g/g in synthetic urine. Water absorption capacity and mechanical performance were modulated by adjusting starch content. Results indicated that oxidized cellulose increased hydrogel pore size within the hydrogel network, while starch functioned as functioned structure backbone, supporting gel integrity. The hydrogels exhibited excellent reswelling properties, losing only 20 to 30% of their initial weight and reabsorbing distilled water over three consecutive reuse cycles. These findings highlight the potential of these sustainable, cost-effective, high-performance hydrogels for personal hygiene, agriculture, and biomedical applications.

Graphical Abstract

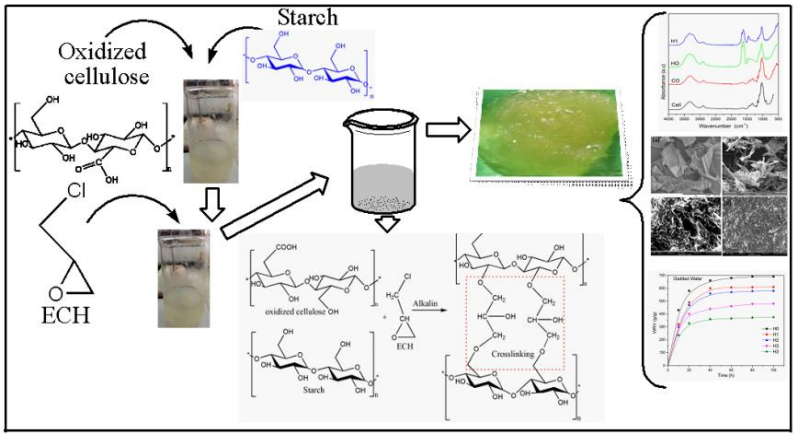

Keywords: Cellulose, Fenton reaction, hydrogels SAPs, Water absorption capacity

1. INTRODUCTION

Superabsorbent polymers (SAPs) are becoming important in engineering fields such as biology, medicine, agriculture and goods consumption due to their high-water absorption capacity [1, 2]. In biological fields, they are used to absorb various liquids, including water, saline solutions, and fluids such as D-glucose and urea solutions. In hygiene products, they are used to manufacture babies diapers and feminine hygiene pads [3]. In the medical field, they are incorporated into hydrocolloid dressings, contact lenses, and drug delivery systems [4]. In agriculture, they are known to be able to improve soil water retention, thereby promoting plant growth [6]. They also find industrial applications in coatings construction materials and chemical absorbents [6]. Traditionally, (SAPs) have been synthesized from petroleum-derived synthetic polymers, which are non-biodegradable and therefore pose significant environmental concerns, particularly in relation to plastic pollution and the increasing challenges of waste management [7, 8]. To address these issues, the replacement of synthetic polymers by modified natural cellulose from lignocellulosic biomass through chemical oxidation processes (e.g., hydrogen peroxide, periodate, TEMPO) has emerged as a promising route to obtain eco-friendly SAPs [9]. Due to its abundance of hydroxyl groups, cellulose is an attractive renewable material for producing high-value functional hydrogels. These hydroxyl groups make cellulose highly reactive, enabling diverse chemical modifications such as oxidation or grafting, which can generate superabsorbent hydrogel materials capable of retaining large quantities of water or solvents [10]. For instance, modified cellulose-based hydrogels can absorb up to four hundred times their dry weight Some investigations have already been conducted on this topic. Investigated on superabsorbent biopolymers (SAPs) prepared from carboxymethylhydroxyethyl cellulose cross linked with divinyl sulfone and they observed that the final material exhibited a significantly high water absorption of about 425 g/g of gel [11]. They attributed this capacity

to the presence of hydrophilic functional groups in their structure, such as hydroxyl (–OH), carboxyl (–COOH), sulfonic ($–SO_3H$), amide ($–CONH_2$), amine ($–NH_3$), and carboxylate ($–COO^-$)[12]. SAP's are typically produced using several methods, including free-radical polymerization, graft polymerization, irradiation crosslinking, physical self-assembly, and more recently. Free-radical polymerization is the most common, involving monomers like acrylic acid and acrylamide, initiated by thermal or chemical agents and cross-linked to form a three-dimensional network[5]. Regarding the Fenton oxidation, which is the focus of this investigation, this method has been used to prepare hydrogels cross-linked with epichlorohydrin (ECH), using hydrogen peroxide as the oxidant and Cu(II) ions as the catalyst. In this reaction medium, the catalyst generates hydroxyl radicals that oxidize cellulose hydroxyl groups into carboxylic acids or aldehydes (hydrophilic functional groups) [13]. Some investigations in the literature have already been made using this approach. For example, Liu *et al.,* (2022) [14] demonstrated that redox initiation using Fe^{2+}/H_2O_2 allows the synthesis of composites from green tea with high swelling capacity and good water retention, achieving a swelling increase of up to 250% compared with untreated counterpart. This work faced some limitations including insufficient control over the oxidation process, which leaded to partial degradation of the biomass. Moreover, the presence of residual iron in the final material was noticed. Liu *et al.*(2023) [14] investigated the Fenton pretreatment of cellulose to enhance its reactivity for superabsorbent polymer (SAPs) synthesis, achieving a 30–40% increase in graft polymerization yield along with higher swelling ratios. The main limitation they faced was the non-selective character of the oxidation that conducted to depolymerization and the challenge of careful removal of residual iron and peroxide to prevent interference in subsequent polymerization. Martinez et *al.,* (2022) [15] employed chelator-mediated Fenton oxidation to selectively oxidize kraft lignin and produce highly hydrophilic, swellable hydrogels, but their study faced challenges in controlling the degree

of oxidation, as well as the heterogeneity, and residual chelator/iron management. The present study focuses on the use of the modified Fenton method that consists of an alkaline metal salt treatment prior to the Fenton reaction on the corresponding cellulose extracted from Corn straw to produce bio-based SAPs. The modification been done to avoid most of the limitations underscored above in other to obtained high yield and strong mechanical modified cellulose materials. Thus, the novelty of the work lies in applying this modified Fenton approach on Corn straw for bio-based SAPs production providing a sustainable pathway to develop bio-based SAPs from agricultural waste [14, 15]. Therefore, the main objective is to extract, purify and chemically modify cellulose from corn straw via Fenton oxidation and then use the modify cellulose to produce high-performance superabsorbent hydrogels and then evaluated their absorption capacities. To achieve this goal, cellulose was extracted from Corn straw using the hot soda process, followed by their bleaching with sodium hypochlorite. The oxidized cellulose was then used to prepare superabsorbent polymers (SAPs) hydrogels through crosslinking with epichlorohydrin (ECH) and then, all the samples were characterized. Cellulose, oxidized cellulose, and crosslinked gels were analyzed using Fourier-transform infrared spectroscopy (FT-IR), thermogravimetric/differential thermogravimetric analysis (TGA–DTG), scanning electron microscopy (SEM), and X-ray diffraction (XRD) and their carboxyl group content in oxidized cellulose and crosslinked gels were determined. The swelling ratios of the hydrogels were evaluated in distilled water, physiological fluids (D-glucose solution and synthetic urine), as well as saline solutions (NaCl, KCl,$CaCl_2$, $AlCl_3$ et $FeCl_3$) and compared to those of commercial materials. Finally, the mechanical properties of the hydrogels were assessed.

2. EXPERIMENTAL SECTION

2.1. Materials

All the reagents used in this study were laboratory grade and were employed without further purification. The plant material selected as the cellulose source was corn straw, chosen for its abundance in Cameroon as an agricultural residue and for the nature of its fibers. The corn straw was collected in the Center Region of Cameroon, in the locality of Etoug-ebe. The harvested material was washed and air-dried at ambient temperature for two weeks. It was then cut into small pieces and ground using a RETSCH mini mill equipped with a 4 mm mesh sieve. Hydrogen peroxide (H_2O_2, 50 wt.%), sodium hydroxide (NaOH, 98 wt.%), hydrochloric acid (HCl, 35 wt.%), and calcium chloride ($CaCl_2$, 99.99 wt.%) were obtained from Sigma-Aldrich. Copper (II) chloride dihydrate ($CuCl_2.2H_2O$ 98 wt.%) was supplied by Merck Darmstadt. Sodium chloride (NaCl, 80 wt. %) was purchased from BDH (British Drug Houses) Chemical Ltd, Poole. Urea ($CO(NH)_2$, 99.9 wt. %) was obtained from Harnstoff. D-glucose ($C_6H_6O_6$, 99 wt. %) was purchased from Merck. Aluminium chloride ($AlCl_3$, 98.5 wt.%) was supplied by Riedel-de Haën. Iron (III) chloride ($FeCl_3$, 45 wt.%) was obtained from Labosi. Epichlorohydrin (C_3H_6Cl 99 wt.%) was purchased from Macros Organics.

2.2. Extraction of cellulose from Corn Straw by the SODA process

Cellulose pulp was obtained from corn straw following an alkaline cooking process with sodium hydroxide[16]. The corn straw powder was treated in a 1 L stainless steel pressurized reactor using a 20% (w/w) sodium hydroxide (NaOH) solution at 150°C for 2 h. The solid-to-liquid ratio was 1 :10 (w/v). After cooking, the mixture was cooled and filtered. The resulting solid residue was washed successively with distilled water and ethanol. Subsequently, a 3% NaOH solution and hydrogen peroxide (H_2O_2) were added directly to

the residue in a 2:1 (v/v) ratio. The mixture was heated at 80°C under constant stirring for 2 h. This operation was repeated three times until a white pulp, corresponding to purified cellulose, was obtained. Next, a 10% (w/w) sodium chlorate solution was introduced into the reaction medium. The mixture was refluxed at 80°C under constant stirring for 2 h. After cooling, the product was washed with distilled water until neutral pH was achieved. The obtained cellulose was dried in an oven at 60°C and stored in a desiccator for further characterization.

2.3. Cellulose Modification

2.3.1. Treatment of Cellulose Pulp with Alkaline Metal Salt Solution

The cellulose pulp was treated with a solution of alkaline metal salts following that the method described by[16] with small modification. Briefly, 10 g of cellulose pulp and 10 g of metal salt (NaCl) were dissolved in 300 mL of distilled water in a 1 L flat-bottomed glass flask equipped with a magnetic stirrer. The mixture was heated under reflux at 80 °C for approximately 7 h, then cooled to room temperature prior to the addition of Fenton oxidation reagents.

2.3.2. Fenton-pulp Modification of NaCl treated cellulose pulp

The cellulose pulp pretreated with NaCl was oxidized using a $H_2O_2 - Cu^{2+}$ system, following by the method described by [16, 17] Typically, 1.5 g of $CuCl_2.2H_2O$ catalyst was directly added to the reaction medium after NaCl treatment. The mixture was stirred at room temperature for 1 h to facilitate the migration of Cu^{2+}ions into the cellulose matrix. The pretreated cellulose was then redispersed in 500 mL of distilled water prior to the addition of H_2O_2 . Subsequently, 500 kg of H_2O_2 (10% w/w) per ton of pulp was slowly added, and the mixture was maintained under stirring at 55 °C for 3 h. Finally, the oxidized cellulose was recovered by vacuum filtration, thoroughly washed with distilled water, and dried in an oven at 60 °C for 24 h.

2.4 Synthesis of superabsorbent hydrogels

Superabsorbent hydrogels were synthesized following the experimental procedure described by [18]. Oxidized cellulose (3% w/w) was dispersed under stirring for 1 h in 97 g of a solution containing 3% (w/w) sodium hydroxide (NaOH), 4% (w/w) urea, and 90% (w/w) water. The mixture was then stored at −15 °C for 24 h. After freezing, the solid was thawed at room temperature and stirred to obtain a clear solution. Starch was dissolved in the same solvent to prepare a solution containing 10 % (w/w) polymers. The oxidized cellulose/starch solutions were mixed in the following mass ratios: 10:0, 9:1, 8:2, 7:3, and 6:4. Subsequently, 5 mL of epichlorohydrin (ECH) was added as a crosslinking agent. The mixtures were stirred at room temperature for 2 h to ensure homogeneity, then heated to 80 °C for 6 h to form hydrogels. Finally, the resulting gels were thoroughly washed with distilled water to remove residual NaOH, urea, and ECH. The hydrogel samples were labeled H0, H1, H2, H3, and H4. The synthesis parameters and operational conditions are summarized in Table 1.

Table 1 : Superabsorbents hydrogels synthesis parameters and preparation conditions.

Samples	Mass of Oxidized Cellulose (3% w/w)	Mass of Starch (3% w/w)	ECH (ml)	Time (h)
H0	100	0	5	6
H1	90	10	5	6
H2	80	20	5	6
H3	70	30	5	6
H4	60	40	5	6

2.5 CHARACTERIZATIONS

2.4.1. Fourier Transform Infrared Spectroscopy (FTIR)

The FTIR spectra of cellulose, oxidized cellulose and the crosslinked gels were recorded on a PerkinElmer Frontier spectrometer equipped with an ATR module (Alphabruker, Nicoled Instrument, USA). The samples were analyzed using the KBr pellets spectra collected in

the wavelength between 4000-400 cm^{-1}, with a resolution of 2 cm^{-1} and 32 scans per spectrum.

2.4.2. XRD Analysis

The crystalline structures of cellulose, oxidized cellulose, and crosslinked gels was characterized by X-ray diffraction (XRD) using an X PERT-PRO (Nicolet Instrument USA) with CuKα radiation (λ = 0.154 nm). The diffraction patterns were recorded over an angular rang 2θ from 10° to 60°, with a scanning rate of 5°/min. The crystallinity of cellulose was determined according to the method described by [19], as expressed in equation (1)

$$\mathrm{CrI(XRD)} = \frac{I_{200} - I_{AM}}{I_{200}} \text{ x } 100 \quad (1)$$

where $I_{(200)}$ denotes the maximum intensity of the diffraction peak associated with the (200) crystalline plane, observed at approximately 2θ = 22.4°, and I(AM) represents the minimum intensity corresponding to the amorphous region, located in the range 2θ = 18.2–18.6°.

2.4.3. Determination of carboxyl group content (TC)

The carboxyl (-COOH) content of oxidized cellulose and crosslinked gels was measured according to the method described [20]. Briefly, 0.5 g of cellulose or hydrogels samples were reacted with 0.01 M aqueous HCl for 1h, followed by thorough washing with distilled water. The obtained samples were dispersed in 50 mL of distilled water, after which 30 mL of 0.25 M aqueous calcium acetate was added. The mixture was stirred for 2 h at room temperature. Finally, a 30 mL aliquot of the supernatant was titrated with 0.01 M NaOH using phenolphthalein (1 wt. % in ethanol) as an indicator. Blank titrations (without sample) were performed to correct the results. The carboxyl (COOH) content was calculated using equation (2).

$$\mathrm{TC}\left(\frac{\mathrm{mmol}}{\mathrm{g}}\right) = \frac{\frac{80}{30} \times 0{,}01\mathrm{M}(V_s - V_b)}{\mathrm{m}} \quad (2)$$

where C_{NaOH} is the NaOH concentration (0.01 M), V_s and V_b are the NaOH Volumes (mL) for the sample and bank, respectively and m is the sample mass (g).

2.4.4. Scanning Electron Microscopy (SEM)

The morphology of cellulose, oxidized cellulose, and crosslinked gels was examined using a Zeiss scanning electron microscope (EBS France). Prior to imaging, all samples were sputter-coated with a thin gold layer to improve conductivity and then examined at 15 kV.

2.4.5. Thermogravimetric Analysis (TGA)

The thermal stability of cellulose, oxidized cellulose, and crosslinked gels was assessed using a thermogravimetric analyzer (TGA UP21, TGA/SDT851, Mettler Toledo, Nicolet Instrument, USA). The measurements were carried out under a nitrogen atmosphere at a heating rate of 10 °C /min and from 30 °C to 600 °C.

2.4.6. Water retention capacity (WRV)

The hydrogels were ground into fine particles and oven-dried at 60 °C for 1h. Then, 0.4 g portion of dried gel was placed in a mesh bag (200 µm) and immersed in 500 mL of distilled water or 0.9 wt. % NaCl solution. At defined time intervals, the bag was removed, hung for 20 min to drain excess liquid, and weighed; the WRV was calculated as equation (3):

$$\mathrm{WRV} = \frac{w_t - w_d}{w_d} \times 100 \quad (3)$$

Where w_t the swollen gel is mass at time *t* and w_d is the initial dry mass. The effect of pH (3-9) on WRV was also evaluated using HCl or NaOH solutions. Swelling in physiological fluids (0.5 wt. % D-glucose, 0.5 wt. % urea, synthetic urine and saline solutions were assessed using the same procedure.

2.4.7. Reswelling kinetics

Reswelling tests in distilled water and 0.9 wt.% NaCl solution were performed after drying the gels at 50 °C for 24 h. Swelling measurement followed the same protocol as section 2.4.6. This dry-swell process constituted one cycle and was repeated three times for each sample.

2.4.8. Measurement of the Sensibility (*f*)

The effect of ions (cations and anions obtained from salts such as NaCl, KCl, $CaCl_2$, $FeCl_3$ et $AlCl_3$) on the swelling rate of hydrogels was investigated following the protocol reported by[21]. The sensibility factor *(f)* of a hydrogel is a dimensionless parameter that quantifies the relative variation of a specific gel property [21] and is defined as shown in equation (4):

$$f = 1 - \frac{W_s}{W_e} \quad (4)$$

where W_e and W_s represent the equilibrium swelling capacities in saline water and distilled water, respectively. All the salts were used at concentrations ranging from 0.01-0.15 mol/L.

2.4.9. Mechanical Testing

The compression resistance of the swollen hydrogels was measured to assess the ability of each material to maintain its structural integrity. The test was made using a universal testing machine (REGGIO Italy). The hydrogels dimensions were 25 mm of diameter (D) and 45 mm in height (H). The initial sample height for compression was 15 mm. Compressive strength σ (kPa) was calculated using equation (5):

$$\sigma = \frac{F}{S} \quad (5)$$

where *F* is maximum fracture force (N) and *S* is the cross-sectional area (mm^2). Each tensile test was repeated three times per sample to ensure result reproducibility.

3. RESULTS AND DISCUSSION

3.1 FTIR analysis

FTIR spectroscopy was used to track the impact of the chemical modification throughout the processing steps (i.e. oxidation, crosslinking, and starch incorporation). Figure 1 presents the FTIR spectra of native cellulose (Cell), oxidized cellulose (CO), and crosslinked hydrogels (HO and H1).

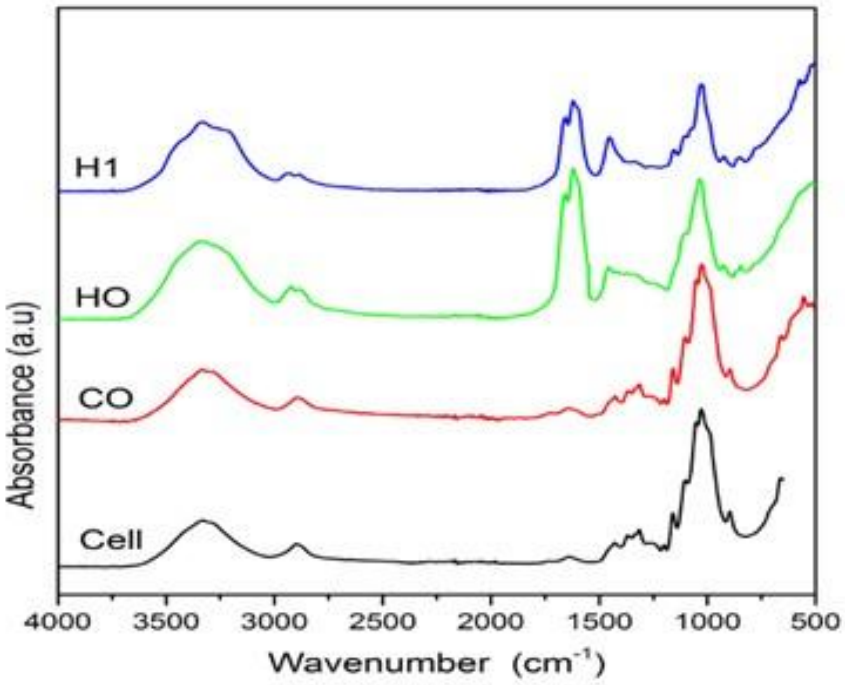

Figure 1: FT-IR spectra of cellulose, oxidized cellulose, and crosslinked gels (HO and H1).

The spectrum of native cellulose (labelled Cell) shows a broad characteristic band at around 3300 cm^{-1}, two small bands at 2900-2830 cm^{-1} and 1030-1015 cm^{-1} corresponding respectively to the stretching vibrations of hydroxyl (-O-H) groups, -C-H vibrations, and the -C-O-C- ether bonds in glycosidic bridges. In additional, addition a band at 895 cm^{-1} is also observed. This is a typical indicator of the β-glycosidic structure of cellulose [22]. Upon oxidation (CO sample), the spectrum shows the appearance of a new band around

1720-1742 cm^{-1} corresponding to carbonyl groups (carboxylic acid aldehydes) resulting from the transformation of hydroxymethyl groups (-CH_2OH) into oxidized groups. The characteristic peaks at 1601 cm^{-1} and 1448 cm^{-1}, observed on the spectrum of all the hydrogel (HO and H1), correspond to the stretching and bending vibration of carboxylate groups (-COO-) [23]. The formation of cross-linked hydrogel without starch (HO) further modifies the spectrum: The -O-H band remains but becomes broader, reflecting the increase in hydrogen interactions that is a sign of the formation of a three-dimensional network[24]. In addition, an intensification of the bands around 1100-1150 cm^{-1} is observed and is a sign of the formation of new -C-O-C- ether bonds between the cellulose chains thanks to epichlorohydrin in an alkaline medium, confirming the presence of cross-linkage within the structure. When comparing sample H1, which contains 10 wt.% of added starch, to HO, the spectrum reveals similarities but also displays some notable differences. The increased intensity of the O–H band is related to starch due to his hydroxyl group. This presence of the starch is also seen via the enhancement of the absorption band between 1020–1040 cm^{-1}, as this corresponds to his glycosidic α-1,4 linkages as reported by Kizil et *al*., (2002) [25].

3.2 Characterization DRX

The Changes in the crystallinity of cellulose, oxidized cellulose, and crosslinked gels were monitored using X-ray diffraction (XRD). The corresponding diffractograms are reported in Figure 2.

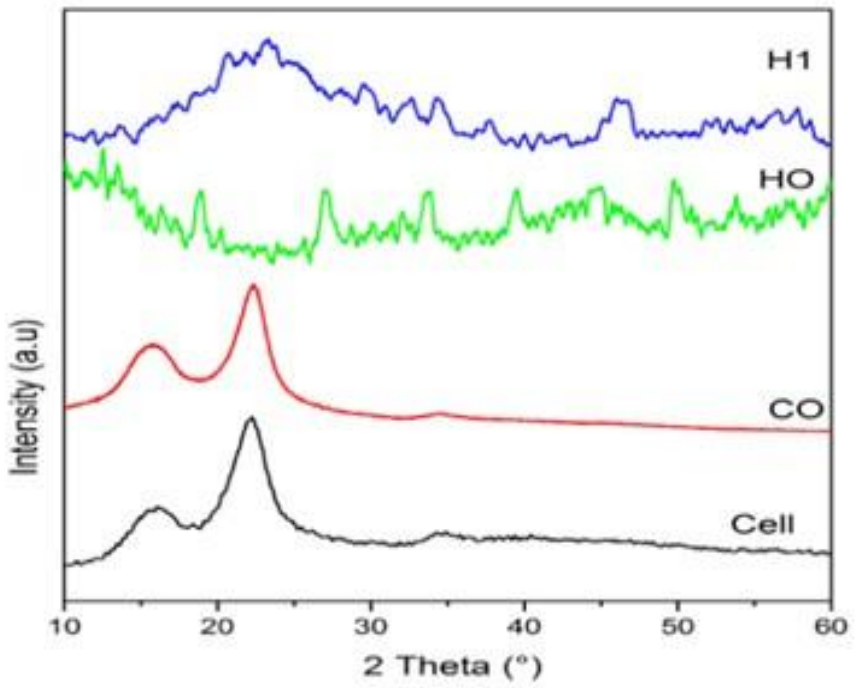

Figure 2 : DRX curve: (a) cellulose (b) Oxidized cellulose (CO) (c) Hydrogel H0 et Hydrogel H1.

Figure 2 shows that cellulose has peaks around 2Θ= 15°, 22°, and 34°, which are characteristic of its semi-crystalline nature [26] . These peaks indicate a well-ordered crystalline structure. Upon oxidation of cellulose (sample CO) these peaks become less intense and broader, particularly around 22°, indicating a reduction of crystallinity. Indeed, using Sergal's [27] method, the crystallinity index (CI) obtained for cellulose pulp is 66.89% and after oxidation, the CI decreases to 59.66%. This can be attributed to the breaking of bonds and the introduction of carboxyl groups. X-ray diffraction (XRD) analysis of the H0 and H1 hydrogels demonstrates the significant influence of starch incorporation on the crystalline architecture of the polymeric matrix. The XRD pattern of the pristine hydrogel (H0) exhibits a broad diffuse diffraction band centered between 2θ = 15° and 22°, which reflects a predominantly amorphous structure resulting from the oxidation of cellulose and its subsequent crosslinking with epichlorohydrin. This reduction in crystallinity is a hallmark of crosslinked cellulose hydrogels, where the crosslinking network disrupts the regular crystalline arrangement of the cellulose chains [28]. Additionally, sharp and high-

intensity diffraction peaks are observed at 2θ = 31.7°, 45.5°, and 56.5–57°, corresponding to the (2.0.0), (2.2.0), and (2.2.2) lattice planes of sodium chloride (NaCl), respectively, indicating the presence of residual salt traces within the matrix [29]. Following the incorporation of starch (hydrogel H1), the diffuse band between 2θ = 15° and 22° becomes noticeably more intense, signifying an enhanced organization of the macromolecular chains and a starch-induced increase in crystallinity. The diffraction peaks associated with the (2.0.0), (2.2.0), and (2.2.2) lattice planes of the residual NaCl (located at 31.7°, 45.5–47°, and 56.5–57°) also become more pronounced. This increase in crystallinity upon starch addition aligns with previous findings reported for cellulose/starch composite hydrogels, where intermolecular interactions between the two biopolymers promote a more ordered structural arrangement [30]. Conclusively, these results indicate that the integration of starch fosters the development of a semi-crystalline framework while preserving the overall amorphous nature of the matrix, which correlates strongly with the observed decrease in the water absorption capacity of H1 compared to H0, as a more ordered and densely packed polymeric network inherently restricts water diffusion into the hydrogel matrix.

3.3 Scanning Electron Micrograph (SEM)

Figure 3 shows the SEM micrograph of cellulose, oxidized cellulose, and crosslinked gels (HO and H1).

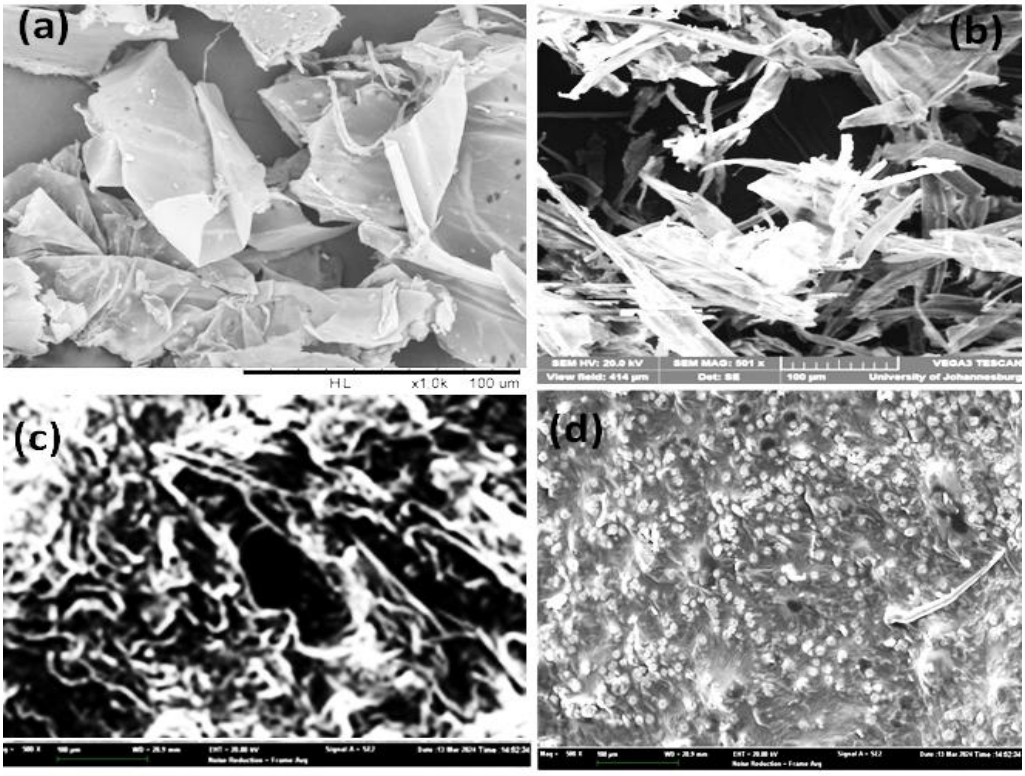

Figure 3: SEM images (a) cellulose (b) Oxidized cellulose (c) crosslinked gels HO et H1.

Figure 3a, illustrates morphology of the neat cellulose surface shows a network of well-defined microfibrils, arranged in a dense and orderly manner. The surface appears fibrous, with smooth and relatively flat regions, reflecting the compact and organized stacking of the cellulose microfibrils. After the oxidation (Figure 3b), the structure becomes more fragmented and disorganized while the fibers show breaks and disintegration of the matrix, indicating an opening of the structure probably due to the introduction of functional groups (aldehyde or carboxyl) during Fenton oxidation [31]. Figure 3c reveals that the HO hydrogel has a highly porous surface with a microporous architecture that can be, but not only, due to the electrostatic repulsion caused by the ionic nature of the carboxylate anion (COO^-) in the HO hydrogel that has increased the space in the cross-linked hydrogel network. Figure 3d reveals an irregular porous structure with a pronounced distribution of micropores of varying sizes. The irregular surface and pores observed, are formed unevenly, probably due to the crosslinking of ECH in the starch as IR- FT data session 3.1 have shown

the possible presence with the structure. As the starch content increases, the pore size decreases, leading to a less open and denser structure compared to HO hydrogel. Indeed, according to Zhou et *al*., (2025) [32], during cross-linking, small starch particles infiltrate the spaces between the polymer network chains, thereby reducing the space available for pore formation. In addition, starch can form bonds with the hydroxyl groups of oxidized cellulose, contributing to the formation of a denser network.

3. 4. Thermogravimetric analysis

The thermal stability of cellulose, oxidized cellulose, and crosslinked gels (HO and H1) was studied via thermogravimetric analysis. The corresponding thermogravimetric (TGA) and derivative thermogravimetric (DTG) thermograms are shown in Figure 4.

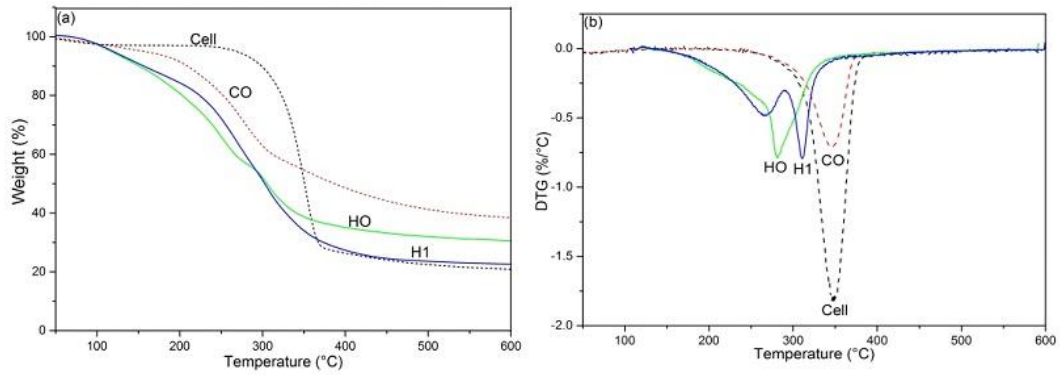

Figure 4. (a) TGA and (b) DTG curves of cellulose (black line), Oxidized cellulose (red line), crosslinked hydrogels (H0 (green line) and H1 (blue line).

The TGA curve shows that native cellulose (Cell) exhibits two mass losses. The first mass loss occurs between 50°C and 110°C and is due to the evaporation of moisture weakly bound to the surface of the materials [33]. The second mass loss begins at around 300°C for cellulose pulp, with maximum degradation observed around 350 °C and is more visible on

the DTG curve (Figure 3b). This mass loss is attributed to the degradation of the macromolecular components of the pulp (cellulose, residual hemicelluloses). Following oxidation (CO), the onset of degradation occurs at slightly lower temperatures, beginning around 250 °C, with a maximum rate of mass loss on the DTG curve near 350 °C. This shift is attributed to the formation of thermally unstable carboxyl groups, which increase the heat sensitivity of the cellulose structure. For HO hydrogel, an initial loss of mass is observed below 150°C, attributed to the loss of free and bound water. Then, a second degradation phase is observed between 250–310°C. According to Arévalo et *al*. (2010) [34], this second degradation phase corresponds to the decomposition of the cross-linked polymer network. When 10% starch is added (H1), the thermal profile slightly changes. Degradation occurs at lower temperatures, between 260°C and 290°C. This behavior indicates that the incorporation of starch slightly reduces the thermal stability of the material. This observation is consistent with the IR-FT and SEM analyses, both of which indicate that starch incorporation decreases the crystallinity of the cellulose network and enhances the porous structure of the resulting hydrogels. The decrease in stability is related to the early onset of starch degradation, which typically begins around 280 °C. Consequently, the presence of starch lowers the thermal breakdown temperature of the hydrogel. This phenomenon was also observed and reported by Pigłowska et al. (2020) [35].

3.5. Swelling properties

3.5.1. Recirculation of superabsorbent hydrogels

The pre-treatment of cellulose with NaCl (activating agent) followed by the Fenton oxidation (Cu^{2+}/H_2O_2) oxidation at a load of 500 kg/t of pulp resulted in the introduction of a carboxylic acid content of 0.48 mmol/g due to the cross-linking mechanism that increase the density of the available active sites. Figure 5 illustrates the proposed cross-

linking mechanism between oxidized cellulose and starch, using epichlorohydrin (ECH) as a cross-linking reagent.

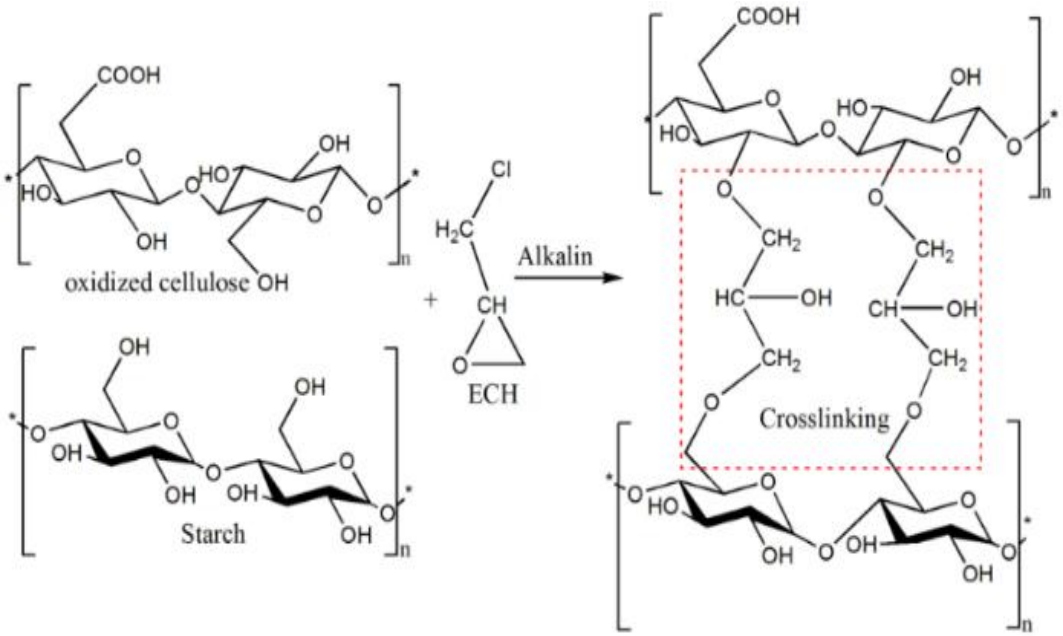

Figure 5. Proposed Cross-linking mechanism.

Based on the work of Chang et *al*. (2010) and Kartha & Srivastava, (1985) [36, 37], the reaction mechanism illustrated in Figure5 shows that the formations of a cross-linked network between oxidized cellulose, starch and epichlorhydrin under alkaline conditions is made by an initial activation of the hydroxyl groups (-O-H) of cellulose and starch through deprotonation that generates high nucleophilic alkoxides. Then, the obtained alkoxide groups react with the electrophilic epoxide ring of ECH leading to its opening and the formation of new ether bond (C-O-C) which presence was confirmed by IR-FT bands between 1100-1150 cm^{-1} (see session 3.1). Since epichlorohydrin possesses two reactive sites, it can establish bridges between different cellulose and starch chains, thereby creating a three-dimensional network.

3.5.2. Chemical composition of hydrogels SAP

The reaction conditions and chemical compositions of the oxidized cellulose and starch hydrogels are shown in Table 2.

Table 2 : Chemical composition of hydrogels.

Samples	Oxidized cellulose content (3% wt. %)	Starch content (3% wt. %)	Group COOH (mmol/g)
H0	100	0	1.33
H1	90	10	1.03
H2	80	20	0.97
H3	70	30	0.88
H4	60	40	0.82

Table 2 shows that HO hydrogel, without starch, containing 100 wt.% oxidized cellulose, has a high carboxyl group content (1.33 mmol/g) and exhibits the highest water retention capacity (WRV) of 691 g of water per gram of gel (noted 691 g/g) in pure water and 113 g/g in saline solution. When 10% starch (H1) is added, there is a slight decrease in water retention capacity (610 g /g and 107 g/g in saline solution), which indicates a synergistic effect between cellulose and starch. However, as the content increases (H2 to H4), there is a gradual decrease in COOH groups, from 0.97 to 0.82 mmol/g, accompanied by a decrease in water retention capacity from 580 to 375 g/g in pure water and from 107 to 80 g/g of gel in the saline solution. This result shows that the addition of starch leads to a reduction in solvent retention. This can be explained by the formation of a denser macromolecular network, reducing the available capillary space, depending on the initial starch content. The cross-linked network structures effectively protected the interior of the gels from the incoming water flow, limiting the hydration of cellulose molecules [38, 39].

3.5.3. Swelling properties in saline solution

The capacity of the hydrogels produced toward water was evaluated and the results of the corresponding kinetic in two swelling media (distilled water and 0.9% NaCl solution) are presented in Figure 6.

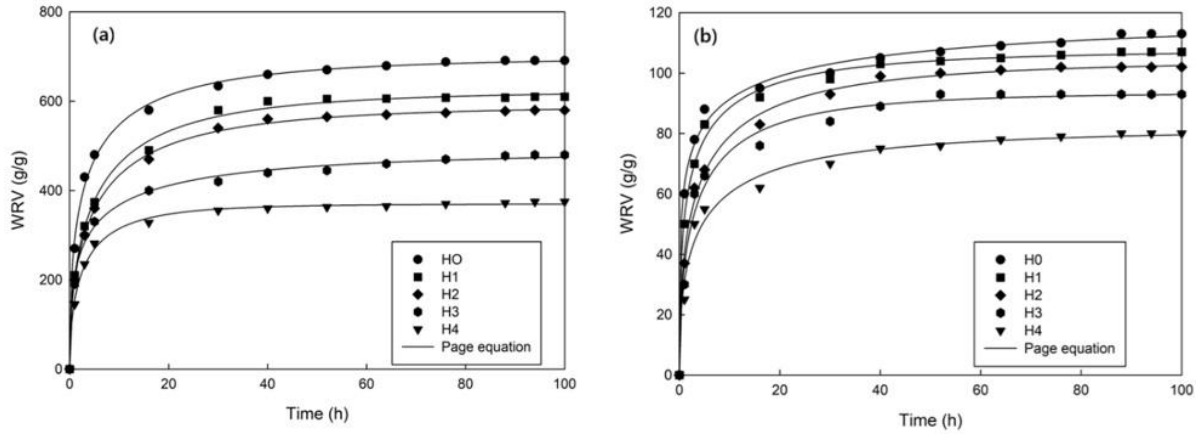

Figure 6: Absorption kinetics of superabsorbent hydrogels with different percentages of starch in distilled water (a) and saline solution (b). The solids lines represent de fitting using the page equation (Equation 6).

Figure 6 shows that the absorption of all the hydrogels, in both solutions, follows a two-step kinetics process. The first step is rapid swelling phase between 0 – 20 h where the swelling rate of hydrogels increases significantly, reflecting rapid absorption of liquid by the polymer networks, and the second phase above 20 h, where progresses more slowly toward a steady state for all the samples. To make a quantitative comparison between the capacity of each sample, a fitting using an empirical drying kinetics model proposed by Page (Equation 6) is applied [40, 41]:

$$\frac{MC\ (t)-M_e}{M_0-M_e} = e^{(-k*t^n)} \qquad (6)$$

Where MC (%) is the water content at time t, Mo (%) is the initial water content, M_e (%) is the saturation water content. According to Simpson et *al. 2017*.[40] (annéeà *k* is the diffusion coefficient and *n* is related to the type of diffusion (*n*>1 super diffusion and *n*<1 a sub diffusion). The fitting of using *Equation 6* to the experimental data was performed using Sigma Plot v.11. Since the materials were dried prior to the beginning of the absorption test,

the initial moisture was considered to zero for all the samples. Figure 6 shows that *Equation 6* can well represent the data as for all the samples, the R^2 obtained after the fitting are greater than 0.99 and the P value less that 0.0001, showing that this drying model can also be considered to the absorption process. The model fitting parameters are reported in Table 3.

Table 3 : Parameters of the Page model (Equation 6) after the fitting

Samples	Solution	M_e (g/g)	M_o (g/g)	k (h^{-1})	n (-)	R (-)
H0		698.91	0	0.534	0.456	0.998
H1		622.64	0	0.399	0.527	0.998
H2	Distilled	589.62	0	0.407	0.514	0.999
H3		490.01	0	0.557	0.396	0.997
H4		369.92	0	0.537	0.547	0.998
H0		119.78	0	0.747	0.284	0.997
H1		107.68	0	0.663	0.415	0.998
H2	Saline	104.10	0	0.487	0.465	0.998
H3		93.52	0	0.491	0.504	0.993
H4		81.43	0	0.481	0.447	0.992

Table 3 shows that in water as solution, the saturation water content (M_e) is completely dependent on the starch/oxidized cellulose quantity in the sample formulation. H0 that contains 100 wt.% of cellulose, without starch exhibited a high quantity of COOH group and thus, absorbed the most (around 698 g/g at equilibrium). When 10 wt. % of starch is added to the composition (Hydrogel H1), the corresponding hydrogel exhibits a reduction of the saturation water by about 10.9% compared to HO, showing that the presence of starch reduces the absorption of the hydrogel. The conjunction of at least the two factors reported below can be explained this trend:

- The introduction of starch reduces the among of oxidized cellulose traduced by the reduction of the among of hydrophilic COOH from 1.33 mmol/g to 1.03 mmol/g (see table 2).
- The presence of the starch particles acts as additional cross-linking points in the hydrogel network via hydrogen bond-type interactions with functional groups in

the matrix, thereby reducing the available active sites that are responsible of the water molecules fixation [42].

As the starch content increases to 20, 30, and 40 wt.%, the corresponding hydrogels (H2–H4) exhibit a progressive decrease in saturation water content, by approximately 15.6%, 29.8%, and 47.1%, respectively. This result confirms the previous observation and shows that an increase in the amount of starch leads to more intermolecular bonds, creating a denser network structure that blocks and/or hinders hydrophilic sites and, thus, limits water absorption. Furthermore, this effect is coupled with the reduction of the quantity of oxidized cellulose in the composition confirmed by the reduction of COOH reported in Table 2. The *Me* value of each hydrogel sample in distilled water is low compared to those of commercial synthetic superabsorbent that is evaluated at approximately 1000 g/g [43]. The diffusion coefficient K reflects how quickly water penetrates a material. This value is slightly higher for the oxidized cellulose hydrogels (H3, H4), traducing a more rapid penetration compared to that of HO even though they absorbed less (low *Me*). This is consistent with the SEM (see session 3.3) as a more porous structures were reported for these samples. The values of *n* for all the oxidized samples were lower than one, showing that all the diffusion processes in the samples were sub-diffusion. Regarding the saline solution Table 3 shows that when compare the same sample (like H0) in water and in saline water) it appears that the saturation content (M_e) is always higher in distilled water than in saline solution. This can be explained by the addition of a third factor to the two previous ones mentioned above and that is the presence of Na^+ and Cl^- ions in the 0.9% NaCl solution. Indeed, these ions contribute to a significant reduction of the swelling capacity due to their electrostatic shielding effect that limits the interaction between hydrophilic groups and water molecules[44]. Moreover, Gupta et *al*. (2012)[45] reported that this behavior can also be attributed to the osmotic pressure generated by the uneven distribution of ions between the external medium and the polymer

network containing Na^+ and Cl^- ions. The presence of Na^+ ions in the surrounding solution reduces this osmotic pressure, leading to a decrease in the driving force for water uptake. As a result, the osmotic swelling caused by the counter-ion imbalance between the gel phase and the solution phase is diminished, thereby lowering the overall capacity. When compared the value of *Me* for each hydrogel in the saline solution, the data in table 3 show that the increase in starch content in the hydrogel also causes the trend observed in water that is a decrease of *Me*, with a slightly lower value when comparing identical samples. After the increase of the quantity of starch in the composition, the value of *Me*, is lowered of about 10.1, 13.1, 21.9 and 32.1% for H1, H2, H3 and H4 compared to H0. Thus, the presence of starch also accentuated the three factors underscore below that lead to the further reduction trend of *Me* reported. As in the case of distilled water, the value of the diffusion coefficient *k* decreases with the presence of starch while that of *n* is lower than one for the hydrogels in saline solutions traducing a less rapid penetration of the saline via diffusion processes that is a sub-diffusion.

3.5.4. Swelling properties of biological solutions on the swelling rate

The water absorption capacity of the samples was also evaluated by determining their equilibrium swelling rate in various aqueous media: distilled water, 0.5% (w/w) D-glucose solution, 0.5% (w/w), urea solution, physiological NaCl saline solution 0.9% (w/w) and a synthetic urine solution containing: 0.8% (w/w) NaCl, 0.1% (w/w) $MgSO_4$, 2% (w/w) urea, and 0.02% (w/w) $CaCl_2$. The data obtained are shown in Figure 7.

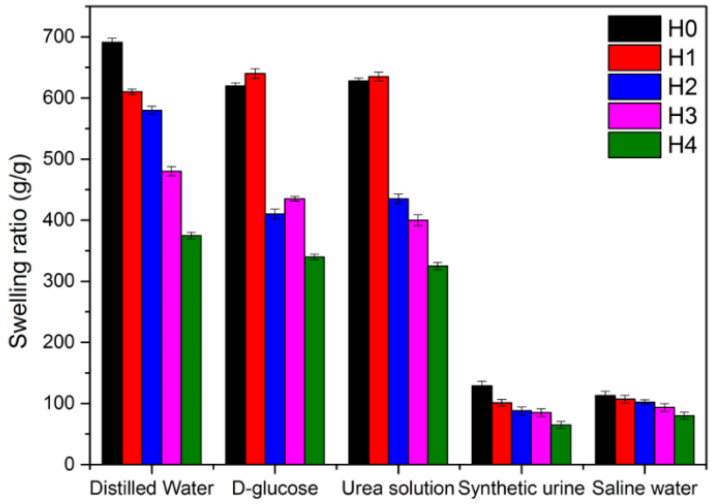

Figure 7 . The effects of biological solutions on the swelling rate of oxidized cellulose/starch hydrogels.

Figure 7 shows that in D-glucose and urea solutions, the swelling rate remains constant, reflecting a low influence on the swelling medium. This could be explained by the weakly ionic nature of these solutions, where the polar groups of the hydrogels interact via the formation of hydrogen bonds as observed by León et *al*., (2019) [46]. On the other hand, immersion in saline solution or synthetic urine leads to a significant decrease in the swelling rate, from 129 to 65 g/g in synthetic urine and from 113 g/g to 80 g/g in saline solution. This reduction can be explained by a filtering or ionic screen effect linked to the presence of cations ($Na^+, K^+, Mg^{2+}, Ca^{2+}$) which attenuate the electrostatic interactions between the (COO^-) groups of cellulose, thereby reducing repulsion and limiting the expansion of the polymer network. Furthermore, the presence of multivalent ions promotes ionic cross-linking. Ionic cross-linking stabilizes the gel but can reduce swelling if the network becomes too right between molecular chains, strengthening the compaction of the network and reducing its swelling capacity[47, 48]. Finally, equilibrium swelling rates also vary between samples. For example, sample HO has a swelling rate between 691 and 645 g/g in distilled water, as well as in D-glucose and urea solutions. In contrast, for sample H4

containing with 40 wt.% starch, exhibits a decrease in the swelling rate, from 348 g/g to 375 g/g. Similar behavior was observed in NaCl and synthetic urine saline solutions.

3.5.5. Effect of salinity on SAP swelling behavior

The salt solutions with the same chloride anion (NaCl, KCl, $CaCl_2$, $FeCl_3$ and $AlCl_3$) were used to evaluate the swelling capacity of the hydrogels. Their effects of different concentrations and types of saline solution on the equilibrium swelling rates of hydrogels are shown in Figure 8.

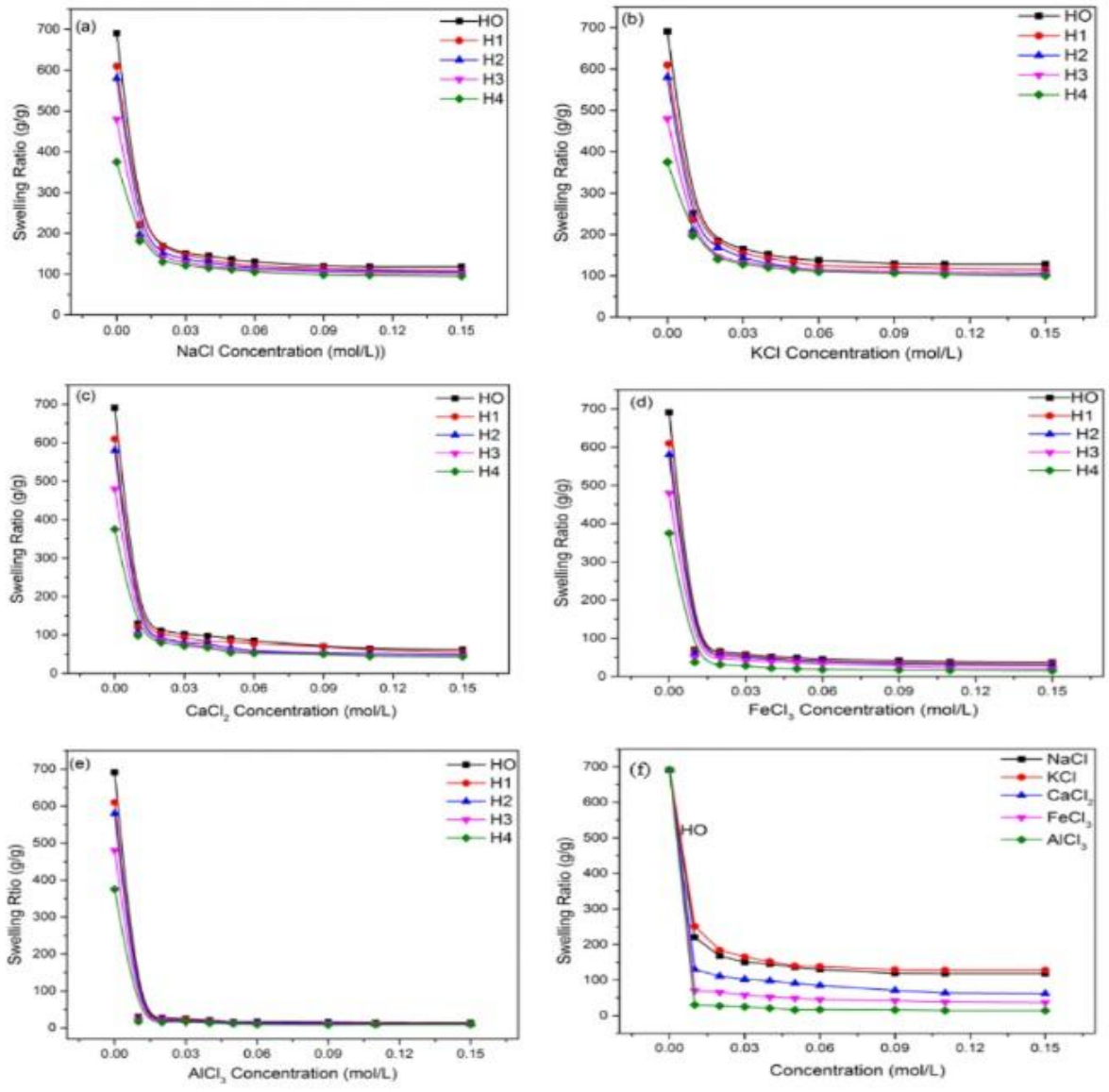

Figure 8 . Influence of metal cations on the swelling capacity of hydrogels

Figure 8 reveals that the swelling rate of hydrogels gradually decreases as the salt concentration increases, stabilizes around 0.02 mol/L. For NaCl and KCl solutions (Figures 8a and 8b), this decrease can be related to the ionic strength of the solution. Hydrogels with starch show a masked reduction in swelling as a function of salt concentration, and particularly with NaCl and KCl. A similar trend is observed with $CaCl_2$, (Figure 8c). However, a more pronounced decrease is noted in media containing $FeCl_3$ and $AlCl_3$ (Figure 9d and 9e), which could be explained by the high valence of the Fe^{3+} and Al^{3+}cations, that facilitate the building of a network establishing bonds with the carboxyl groups of oxidized cellulose via cross-linking. According Barbucci et *al*. (2000)[23], the cross-linking capacity increases with the valence and polarizing power of the cations, thus influencing the behavior of superabsorbent polymers. Moreover, Castel et *al*.(1990[49]) pointed out that trivalent cations exert a higher ionic strength than di- or monovalent cations ($Na^+$and K^+), resulting in a significant decrease in swelling rate. Mobile ions and their valence or oxidation state are both responsible for ionic strength (Figure 8f). As a result, a small amount of monovalent ($Na^+$and K^+), divalent (Ca^{2+}), and trivalent (Fe^{3+} and Al^{3+}) ions can significantly reduce swelling values. This phenomenon led to the reduction in electrostatic repulsion between polyionic chains due to the neutralization of negative charges, leading to additional cross-linking of the network. In addition, the possibility of complexation between carboxylate groups and trivalent cations induces the formation of intra- and intermolecular structures, that can further limit gel expansion (Figure8). Finally, this behavior also depends on the ionic radius. Indeed, a cation with a larger ionic radius restricts the infiltration of water into the polymer network, thereby reducing the overall water absorption of the gel [50, 51]. Thus, the swelling trend observed here can be attributed to a synergistic effect of all the mechanisms discussed above, as the conditions required for each phenomenon to occur are fulfilled (Figure 9).

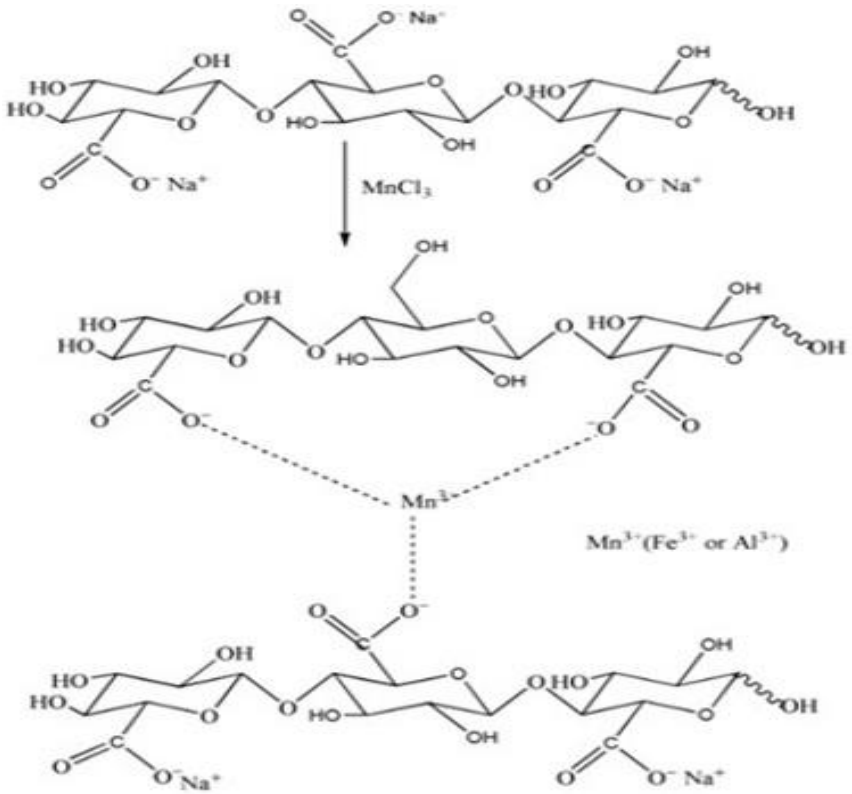

Figure 9 . Complexation of carboxylate groups with trivalent cations.

3.5.6. Effect of sensitivity factor (*f*) on equilibrium swelling rate

The ability of hydrogels to absorb water depends heavily on the nature of the ions present in solution. The specific effect of a type of ion on swelling can be quantified by the sensitivity factor *(f)*, which varies from one salt to another in function of the hydrogel's response to environmental variations, such as ionic strength [52]. The data in Table 3 indicate that the higher the absorption capacity (M_e) of a hydrogel, the lower the sensitivity factor *(f)*, reflecting an inverse relationship between these two parameters. Thus, salts that significantly alter the ionic strength of the medium cause a marked reduction in swelling. The results show that Fe^{3+} and Al^{3+} salts are associated with higher sensitivity factors than divalent or monovalent salts such as $CaCl_2$, NaCl, and KCl. This is explained by the low cross-linking capacity of Fe^{3+} and Al^{3+} ions with carboxylate groups in the polymer network, which

limits the expansion of the network in saline environments. Conversely, weakly charged ions such as those in KCl or NaCl interact little with the polymer chains and therefore induce low sensitivity.

Table 6. Effect of absorbed metal on the sensitivity factor and swelling capacity of hydrogel soaked for 60 hours (H0) (WRV of 691 g of water/g of gel)

Metal	Concentration (mol/L)	W_s (g /g)	Sensibility factor *(f)*
NaCl	0.01	220	0 .681
	0.03	150	0.782
	0,05	136	0.803
	0.09	119	0.827
	0.11	118	0.829
	0.15	118	0.829
KCl	0.01	251	0.636
	0.03	165	0.761
	0.05	140	0.797
	0.09	129	0.813
	0.11	128	0.814
	0.15	128	0.814
$CaCl_2$	0,01	130	0.811
	0.03	102	0.854
	0.05	91	0.868
	0,09	71	0.897
	0,11	64	0.907
	0.15	62	0.910
$FeCl_3$	0.01	70	0.811
	0.03	58	0.852
	0,05	49	0.868
	0.09	42	0.897
	0.11	38	0.945
	0.15	37	0.946
$AlCl_3$	0.01	30	0.956
	0.03	25	0.963
	0.05	16	0.977
	0.09	16	0.977
	0.11	14	0.979
	0.15	14	0.979

3.5.7. Swelling properties of hydrogels in water at different hydrogen potential (pH) values and mechanical properties of hydrogels SAP

The study of the influence of pH on swelling ratio was conducted at room temperature and constant pressure, and the data are reported in figure 10. The pH values were set between 3 and 9.

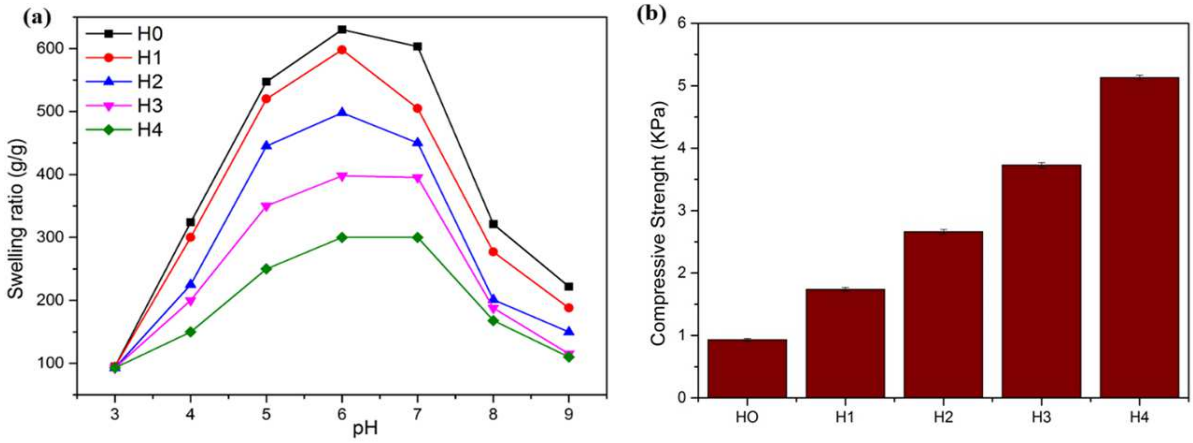

Figure 10 . (a) Influence of medium pH on swelling at different starch contents and (b) Evolution of the compressive strength of hydrogels as a function of starch content.

Figure 10a shows that for pH values below 5, there is a rapid increase in the swelling rate reaching a maximum around this point. Then, when the pH exceeds 5, a decreasing trend of the swelling rate is noticed. This behavior can be due to the protonation of the carboxyl group ($-COO^-$ to -COOH) and their involvement in the cross-linking within the hydrogel through hydrogen bonds formation, making the gel structure more compact and thereby limiting its expansion [53]. The decreasing trend is probably due to a counter-ion effect that reduced the effectiveness of repulsion between negative charges and hindered further expansion. This phenomenon results in a decrease in swelling. All the hydrogels' samples exhibited similar behavior across the entire pH range studied. The maximum of the swelling ratio is 630 g/g, 600 g/g, 500 g/g, 400 g/g and 300 g/g for HO to H4 respectively, traducing decreasing trend that is consistent with the previous observation made a session 3.5.4. The

mechanical properties (compressive strength) of SAPs hydrogels were evaluated at room temperature was measured and the data are reported in Figure12b.The data show that, for the control sample H0, which does not contain starch, has the lowest strength 0.93 kPa. The addition of 10 wt.% starch (H1) results in a slight increase in strength, reflecting the beginning of reinforcement of the hydrogel network structure 1.74 kPa. This improvement becomes more pronounced when the amount of starch is increased to 20% (H2), 30% (H3) and 40 % (H4). Indeed, the mechanical strength of H2, H3 and H4are 2.66 kPa, 3.73 kPa, respectively. These values are respectively, 1.8, 4 and 6 times higher than that of HO confirming the reinforcing effect of starch. This behavior may be related to improved crosslinking density and stronger interaction between oxidized cellulose and starch, making the gel matrix more resistant to mechanical deformation. These results are consistent with the swelling rate of hydrogels reported in this work in sessions 3.5.3 and 3.5.4.

4. CONCLUSION

The study conducted on the extraction and modification of cellulose demonstrated its strong potential as a renewable raw material for the synthesis of superabsorbent polymers, particularly hydrogels. Cellulose pretreated (NaCl) and then oxidized by the Fenton reaction (Cu^{2+}/H_2O_2) through the introduction of carboxyl groups (0.48 mmol/g) showed increased swelling capacity. Its combination with starch strengthened the structure of the network formed, improving mechanical stability and thermal, as demonstrated by mechanical analyses, FT-IR, XRD and SEM. The FT-IR analyses revealed the formation of a network cross-linked by ether bonds. XRD analysis of the cross-linked hydrogels shows the predominance of the amorphous phase. SEM micrographs revealed a highly porous structure, which was reduced with the addition of starch at different concentrations. Thermal analyses showed that the degradation of SAP hydrogels without starch addition occurs at a

lower temperature than that of starch-reinforced superabsorbent hydrogels. The absorption and water retention performance was studied in distilled water, 0.9% NaCl physiological solution, and biological solutions. The absorption and retention capacities decreased significantly in the NaCl solution compared to those obtained in distilled water due to the increase in the ionic strength of the swelling medium. The addition of different starch contents significantly decreases the absorption and retention values in water and biological solutions. SAP hydrogels showed pH values between 5 and 7, where the absorption rate remained almost constant and maximum swelling was extinguished.

Ethics approval and consent to participate

Not applicable

Consent to participate

All authors read and approved the final manuscript

Availability of data and materials

Data available from the corresponding author

Competing interests

The authors declare that they have no competing of interest.

Funding

The Macromolecular Chemistry research unit at the University of Yaoundé I (Cameroon) received help from the Ministry of Scientific Research and Innovation.

Authors' contributions

All authors contributed to study's conception and design.

Material preparation and synthesis were performed by Fabien Lucioni Tsague, Desire Yomeni and Jean-Bosco Saha.

Data collection and analysis were performed by Fabien Lucioni Tsague, Desire Yomeni Cheumani and Jean-Bosco Saha.

The first draft of the manuscript was written by Fabien Lucioni Tsague and all authors commented on previous versions of the manuscript.

Acknowledgements

The authors acknowledge Stenley Olivier Kanemoto and Aime Martial Kuete from the University of Yaoundé I, Macromolecular Chemistry Research Team, for doing the X-ray diffraction, thermal analyses and Scanning Electron Microscopy. They also appreciate the support from the Ministry of Scientific Research and Innovation.

REFERENCES

1. Ahmed EM (2015) Hydrogel: Preparation, characterization, and applications: A review. Journal of advanced research 6:105–121
2. Caló E, Khutoryanskiy VV (2015) Biomedical applications of hydrogels: A review of patents and commercial products. European polymer journal 65:252–267
3. Tuteja J, Vyas A (2023) Progressive approach of SAPs in disposable hygiene industry. In: Properties and Applications of Superabsorbent Polymers: Smart Applications with Smart Polymers. Springer, pp 171–181
4. Rehman WU, Asim M, Hussain S, et al (2020) Hydrogel: a promising material in pharmaceutics. Current Pharmaceutical Design 26:5892–5908
5. Ma X, Wen G (2020) Development history and synthesis of super-absorbent polymers: a review. Journal of Polymer Research 27:136
6. Krasnopeeva EL, Panova GG, Yakimansky AV (2022) Agricultural applications of superabsorbent polymer hydrogels. International Journal of Molecular Sciences 23:15134
7. Zhang Y, Zhu PC, Edgren D (2010) Crosslinking reaction of poly (vinyl alcohol) with glyoxal. Journal of Polymer Research 17:725–730
8. Huettermann A, Orikiriza LJ, Agaba H (2009) Application of superabsorbent polymers for improving the ecological chemistry of degraded or polluted lands. CLEAN–Soil, Air, Water 37:517–526
9. Petroudy SRD, Ranjbar J, Garmaroody ER (2018) Eco-friendly superabsorbent polymers based on carboxymethyl cellulose strengthened by TEMPO-mediated oxidation wheat straw cellulose nanofiber. Carbohydrate polymers 197:565–575
10. Zhang W, Wang P, Liu S, et al (2021) Factors affecting the properties of superabsorbent polymer hydrogels and methods to improve their performance: a review. Journal of Materials Science 56:16223–16242
11. Annergren J, Bragd P, Himmelmann G (2002) Absorbent structure comprising a highly absorbent polymer, and an absorbent article comprising the absorbent structure. Google Patents
12. Sharma K, Kumar V, Chaudhary B, et al (2016) Application of biodegradable superabsorbent hydrogel composite based on Gum ghatti-co-poly (acrylic acid-aniline) for controlled drug delivery. Polymer degradation and stability 124:101–111
13. Yang Q, Adrus N, Tomicki F, Ulbricht M (2011) Composites of functional polymeric hydrogels and porous membranes. Journal of Materials Chemistry 21:2783–2811
14. Liu Y, Zhu Y, Mu B, et al (2023) Fenton-like redox-initiated synthesis of superabsorbent composites with excellent water retention and swelling properties based on green tea and oil shale semi-coke. European Polymer Journal 182:111716
15. Martinez DV, Rodriguez A, Juarros MA, et al (2022) Depolymerization of lignin for biological conversion through sulfonation and a chelator-mediated Fenton reaction. Green Chemistry 24:1627–1643
16. Tsague FL, Chimeni DY, Assonfack HL, et al (2024) Study of oxidation of cellulose by Fenton-type reactions using alkali metal salts as swelling agents. Cellulose 31:6643–6661
17. Xu X, Lu N, Wang S, et al (2021) Extraction and characterization of microfibrillated cellulose from discarded cotton fibers through catalyst preloaded fenton oxidation. Advances in Materials Science and Engineering 2021:5545409
18. Rodhiyah M, Luthfianti HR, Waresindo WX, (2024) Enhanced Superabsorbency of Cellulose-Based Hydrogels in NaOH Solution: Synthesis, Characterization, and Performance Evaluation. In: Journal of Physics: Conference Series. IOP Publishing, p 012036
19. Segal L, Creely JJ, Martin Jr AE, Conrad CM (1959) An empirical method for estimating the degree of crystallinity of native cellulose using the X-ray diffractometer. Textile research journal 29:786–794
20. Alam MN, Islam MS, Christopher LP (2019) Sustainable production of cellulose-based hydrogels with superb absorbing potential in physiological saline. ACS omega 4:9419–9426
21. Spagnol C, Rodrigues FH, Pereira AG, (2012) Superabsorbent hydrogel composite made of cellulose nanofibrils and chitosan-graft-poly (acrylic acid). Carbohydrate Polymers 87:2038–2045

22. Jalbert J, Gilbert R, Tétreault P, et al (2007) Identification of a chemical indicator of the rupture of 1, 4-β-glycosidic bonds of cellulose in an oil-impregnated insulating paper system. Cellulose 14:295–309
23. Barbucci R, Magnani A, Consumi M (2000) Swelling behavior of carboxymethylcellulose hydrogels in relation to cross-linking, pH, and charge density. Macromolecules 33:7475–7480
24. Clegg RS, Reed SM, Hutchison JE (1998) Self-assembled monolayers stabilized by three-dimensional networks of hydrogen bonds. Journal of the American Chemical Society 120:2486–2487
25. Kizil R, Irudayaraj J, Seetharaman K (2002) Characterization of irradiated starches by using FT-Raman and FTIR spectroscopy. Journal of agricultural and food chemistry 50:3912–3918
26. Salem KS, Kasera NK, Rahman MA, et al (2023) Comparison and assessment of methods for cellulose crystallinity determination. Chemical Society Reviews 52:6417–6446
27. Segal L, Creely JJ, Martin Jr AE, Conrad CM (1959) An empirical method for estimating the degree of crystallinity of native cellulose using the X-ray diffractometer. Textile research journal 29:786–794
28. French AD (2014) Idealized powder diffraction patterns for cellulose polymorphs. Cellulose 21:885–896
29. Djouama M (2014) Etude des diagrammes de diffraction des rayons X des composés ioniques de type NaCI
30. Nafisah N, Rodhiyah M, Luthfianti HR, (2024) Enhanced Superabsorbency of Cellulose-Based Hydrogels in NaOH Solution : Synthesis, Characterization, and Performance Evaluation. In: Journal of Physics: Conference Series. IOP Publishing, p 012036
31. Gohil JM, Bhattacharya A, Ray P (2006) Studies on the crosslinking of poly (vinyl alcohol). Journal of polymer research 13:161–169
32. Zhou D, Li D, Liu M, et al (2021) Experimental parameters affecting cross-linking density and free-thaw stability of cross-linked porous starch. ES Food & Agroforestry 5:20–28
33. Poletto M, Ornaghi Junior HL, Zattera AJ (2014) Native cellulose: structure, characterization and thermal properties. Materials 7:6105–6119
34. Arévalo R, Picot OT, Wilson RM, et al (2010) All-cellulose composites by partial dissolution of cotton fibres. Journal of Biobased Materials and Bioenergy 4:129–138
35. Pigłowska M, Kurc B, Rymaniak Ł, (2020) Kinetics and thermodynamics of thermal degradation of different starches and estimation the OH group and H2O content on the surface by TG/DTG-DTA. Polymers 12:357
36. Chang C, Duan B, Cai J, Zhang L (2010) Superabsorbent hydrogels based on cellulose for smart swelling and controllable delivery. European polymer journal 46:92–100
37. Kartha KPR, Srivastava HC (1985) Reaction of epichlorhydrin with carbohydrate polymers. Part II. Starch reaction mechanism and physicochemical properties of modified starch. Starch-Stärke 37:297–306
38. Chaudhary V, Sharma S (2019) Suspension polymerization technique: parameters affecting polymer properties and application in oxidation reactions. Journal of Polymer Research 26:102
39. Alam MN, Islam MS, Christopher LP (2019) Sustainable production of cellulose-based hydrogels with superb absorbing potential in physiological saline. ACS omega 4:9419–9426
40. Simpson R, Ramírez C, Nuñez H, et al (2017) Understanding the success of Page's model and related empirical equations in fitting experimental data of diffusion phenomena in food matrices. Trends in Food Science & Technology 62:194–201
41. Tagawa A, Muramatsu Y, Nagasuna T, et al (2003) Water absorption characteristics of wheat and barley during soaking. Transactions of the ASAE 46:361
42. Rashidzadeh A, Olad A, Salari D, Reyhanitabar A (2014) On the preparation and swelling properties of hydrogel nanocomposite based on sodium alginate-g-poly (acrylic acid-co-acrylamide)/clinoptilolite and its application as slow release fertilizer. Journal of Polymer Research 21:344
43. Liu Y, Xie J-J, Zhu M-F, Zhang X-Y (2004) A study of the synthesis and properties of AM/AMPS copolymer as superabsorbent. Macromolecular Materials and Engineering 289:1074–1078

44. Bashir S, Hina M, Iqbal J, et al (2020) Fundamental concepts of hydrogels: Synthesis, properties, and their applications. Polymers 12:2702
45. Gupta NV, Shivakumar HG (2012) Investigation of swelling behavior and mechanical properties of a pH-sensitive superporous hydrogel composite. Iranian journal of pharmaceutical research: IJPR 11:481
46. Leon O, Soto D, Antunez A, et al (2019) Hydrogels based on oxidized starches from different botanical sources for release of fertilizers. International journal of biological macromolecules 136:813–822
47. Zhao Y, Kang J, Tan T (2006) Salt-, pH-and temperature-responsive semi-interpenetrating polymer network hydrogel based on poly (aspartic acid) and poly (acrylic acid). Polymer 47:7702–7710
48. Zhang M, Zhang S, Chen Z, et al (2019) Preparation and characterization of superabsorbent polymers based on sawdust. Polymers 11:1891
49. Castel D, Ricard A, Audebert R (1990) Swelling of anionic and cationic starch-based superabsorbents in water and saline solution. Journal of applied polymer science 39:11–29
50. Kalendova P, Svoboda L, Hroch J, (2021) Hydrogels based on starch from various natural sources: Synthesis and characterization. Starch-Stärke 73:2100051
51. León O, Soto D, Antúnez A, (2019) Hydrogels based on oxidized starches from different botanical sources for release of fertilizers. International journal of biological macromolecules 136:813–822
52. Luo R, Li H (2009) A modeling study of the effect of environmental ionic valence on the mechanical characteristics of pH–electrosensitive hydrogel. Acta biomaterialia 5:2920–2928
53. Duquette D, Dumont M-J (2018) Influence of Chain Structures of Starch on Water Absorption and Copper Binding of Starch-Graft-Itaconic Acid Hydrogels. Starch-Stärke 70:1700271